ACS OMEGA

Article

Cite This: ACS Omega 2019, 4, 10171−10175

http://pubs.acs.org/journal/acsodf

β-As Monolayer: Vibrational Properties and Raman Spectra

Somayeh Saboori,[†] Zexiang Deng,[†] Zhibing Li,*[,†] Weiliang Wang,*[,†] and Juncong She[‡]

[†]State Key Laboratory of Optoelectronic Materials and Technologies, Guangdong Province Key Laboratory of Display Material and Technology, School of Physics, Sun Yat-sen University, Guangzhou 510275, People's Republic of China

[‡]State Key Laboratory of Optoelectronic Materials and Technologies, Guangdong Province Key Laboratory of Display Material and Technology, School of Electronics and Information Technology, Sun Yat-sen University, Guangzhou 510275, People's Republic of China

ABSTRACT: Recently, semiconducting and other extraordinary properties of the monolayer of the V-group element have attracted a broad interest and attention. The success of experimentally growing antimonene and black phosphorus makes the arsenic monolayer a reasonable candidate for two-dimensional semiconductors. By using DFT calculation, we investigate the vibrational properties and Raman spectra of the buckled honeycomb monolayer of arsenic (β-As) for four commonly used laser lines. By calculating Raman tensor of each active modes of the β-As monolayer, we obtained polarization angle-dependent Raman intensities when the wave vector of incident light is parallel and perpendicular with the plane of the β-As monolayer. We found that the nonresonant Raman spectra have two peaks at 235 and 305 cm^{-1} that correspond to the in-plane vibrating mode E_g and out-of-plane vibrating mode A_{1g}, which is similar to germanene, blue phosphorene, and β-Sb monolayer Raman spectra. There are two (four) minima and two (four) maxima when the polarization direction of scattered light is parallel (perpendicular) to that of the incident light and the wave vector of the incident light is parallel to the β-As monolayer. The Raman intensities of neither parallel polarization configuration nor perpendicular polarization configuration depend on the polarization direction when the wave vector of incident light is perpendicular to the β-As monolayer. The relation between shapes of the polar plots and relative values of Raman tensor elements is found. The Raman intensities decrease with increasing wavelength of incident laser lines in most cases. Our results will help experimentalists to identify the existence and the orientation of the β-As monolayer while they are growing the β-As monolayer.

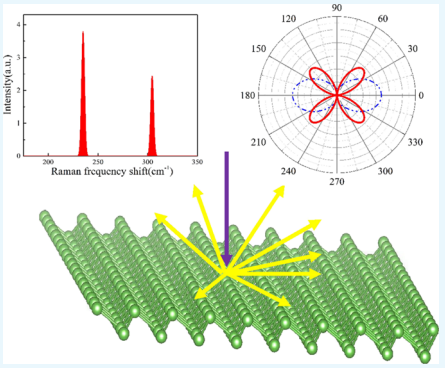

INTRODUCTION

Recently, few-layered structures of group-V element have attracted much attention in the nanoelectronic and optoelectronic fields. Black phosphorene, a monolayer of phosphorus atoms, is a popular member of this group because of having extraordinary properties such as direct moderate band gap,[1] high carrier mobility,[2] and anisotropic[3] transport properties. Blue phosphorene is another allotrope of phosphorene. The growth of blue phosphorene on Au(111) was reported by using a molecular beam epitaxial, in 2016.[4] The high thermal conductivity[5,6] and large band gap of blue phosphorene are one of the features that makes it a good suggestion for the electronic industry.[7,8] Lei et al. succeeded to experimentally grow antimonene, which is another member of group-V, on Bi_2Te_3 and Sb_2Te_3.[9] Comparing with group IV (graphene,[10] silicene,[11] etc.), this group has a large band gap in their few layer structures, that is, an indispensable feature in electronic applications.

The gray arsenic, yellow arsenic, and black arsenic are the three common allotropes of arsenic.[12] The bulk of gray arsenic is semimetal. The existence of monolayer and bilayer of gray arsenic has been predicted because of its weak interlayer interaction.[13−15] The band gap of gray arsenic changes from ∼0.175 to ∼2.49 eV when its thickness decreases from bulk to monolayer.[16−18] The buckled and puckered honeycomb structures are two stable monolayers of arsenic that are also called β-arsenene and α-arsenene, respectively. The α-arsenene was predicted[13,19] to be a semiconducting material with a direct band gap and has high carrier mobility[20] and strong anisotropy.[20] The structure of β-arsenene with an indirect band gap is similar to that of the layered blue phosphorus; this structure is a little more stable than that of α-arsenene.[13] The investigated optical properties show that β-arsenene could be very useful in various photovoltaic and optoelectronic applications.[14]

Although few-layer arsenic has not been experimentally studied yet,[13] the success of growing antimonene,[9] black phosphorene,[21] and blue phosphorene[4] makes arsenic monolayers plausible candidates for two-dimensional (2D) semiconductors.

Up to now, there is not any study about vibrational properties and Raman spectra of the β-As monolayer, which is essential for the experimentalists to investigate the electronic and thermal properties of graphene and beyond,[22] and to

Received: March 14, 2019
Accepted: May 29, 2019
Published: June 12, 2019

DOI: 10.1021/acsomega.9b00712
ACS Omega 2019, 4, 10171−10175

identify the β-As monolayer when experimentalists are trying to grow it. Raman spectroscopy is also possible to determine the pressure by measuring the blue shift of Raman optical modes.[23] In this work, we investigated vibrational properties of the β-As monolayer, based on the density functional theory (DFT) calculation. We calculated Raman tensor and thus the polarization direction-dependent Raman intensities of the β-As monolayer with four commonly used laser lines (532, 633, 830, and 785 nm).

RESULTS AND DISCUSSION

The phonon dispersion curve (Figure 1b) of the β-As monolayer (Figure 1a) shows that there is no imaginary

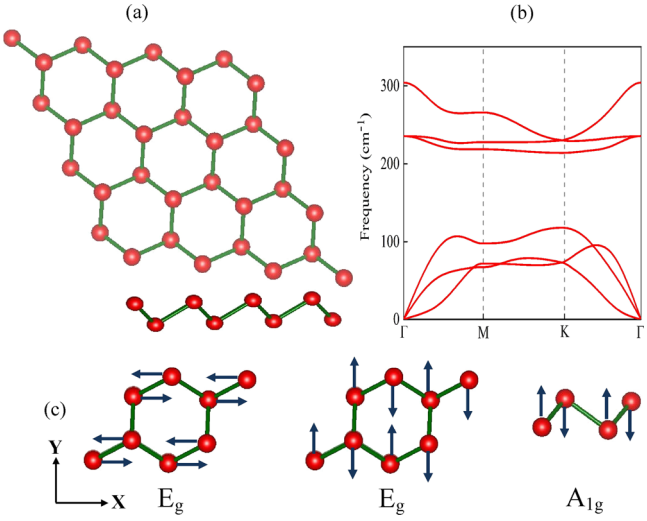

Figure 1. (a) Top and side view of 3 × 3 × 1 β-As monolayer (buckled monolayer arsenic), (b) Phonon dispersions of β-As monolayer, and (c) Raman active modes A_{1g} (out-of-plane) and E_g (in-plane) at Γ point.

vibrating mode which means that the β-As monolayer has the dynamic stability. There are 3 optical modes. All of them are Raman active. The phonon dispersion is similar to those of blue phosphorene[24] and β-antimonene.[25] Our result also agrees with the previous work.[19]

The β-As monolayer belongs to the D_{3d} point group, whose Raman active modes are A_{1g} and E_g (doubly degenerate). The A_{1g} mode is out-of-plane vibration (Figure 1c) whose frequency is 305 cm^{-1}. The E_g (doubly degenerate) mode is in-plane vibration (Figure 1c) whose frequency is 235 cm^{-1}. Table 1 lists the Raman-active modes and the Raman shifts of β-As monolayer, germanene, blue phosphorene, and β-Sb monolayer. All of these four materials belong to space group $P\bar{3}m1$ and point group D_{3d}.

Table 1. Raman Active Modes and the Corresponding Raman Shifts (in cm^{-1} Unit) of β-As Monolayer, Germanene, Blue Pohosphorene, and β-Sb Monolayer

materials	A_{1g}	E_g
germanene[24]	160	310
blue pohsphorene[24]	550	435
β-As monolayer (present work)	305	235
β-Sb monolayer[25]	195	150

We considered four commonly used laser lines with wavelengths 532, 633, 785, and 830 nm, corresponding to photon energies of 2.33, 1.96, 1.57, and 1.49 eV, respectively. Two of them are larger than the band gap of the β-As monolayer 1.59 eV,[26] two of them are smaller than the band gap. This band gap is underestimated by DFT and can be improved by hybrid exchange−correlation functional[26] or exchange−correlation energy whose derivative of the density (or density matrix) with respect to the number of electrons is discontinued at integers.[27,28]

After finding the Raman tensor, we calculated the Raman intensity; we considered that the β-As monolayer is in xy plane. Therefore, the incident light is parallel to the β-As monolayer plane when the incident light wave vector is along x-axis. The polarization direction of the incident light can be written as $e_i = (0, \cos\theta, \sin\theta)$; it is a common practice to measure the parallel and perpendicular polarized scattered light whose polarization direction is $e_s^{\parallel} = (0, \cos\theta, \sin\theta)$ and $e_s^{\perp} = (0, -\sin\theta, \cos\theta)$, respectively. These are called parallel polarization configuration and perpendicular polarization configuration, respectively.

The form of Raman tensors we obtained agrees with the group theory. β-As belongs to the D_{3d} point group. The Raman tensor of their Raman-active modes A_{1g} and E_g (doubly degenerate) modes has the form[29]

$$\tilde{R}(A_{1g}) = \begin{pmatrix} a & 0 & 0 \\ 0 & a & 0 \\ 0 & 0 & b \end{pmatrix}$$

$$\tilde{R}(E_{g,1}) = \begin{pmatrix} c & 0 & 0 \\ 0 & -c & d \\ 0 & d & 0 \end{pmatrix}$$

$$\tilde{R}(E_{g,2}) = \begin{pmatrix} 0 & c & d \\ c & 0 & 0 \\ d & 0 & 0 \end{pmatrix} \quad (1)$$

where a, b, c, and d are main terms, other elements are 0 because of the point group symmetry. By substituting the calculated Raman tensor for each modes and polarization vectors of the incident and scattered light into eq 11 in the Methods section, we have calculated the polarization angle-dependent Raman intensity for each mode. The Raman intensities for these two polarization settings are

$$I^{\parallel}(A_{1g}) \propto |a|^2\cos^4\theta + |b|^2\sin^4\theta + 1/2\ \mathrm{Re}(a\cdot b^*)\ \sin^2(2\theta) \quad (2)$$

$$I^{\parallel}(E_g) \propto |c|^2\cos^4\theta + |d|^2\sin^2(2\theta) - 2\ \mathrm{Re}(c\cdot d^*)\cos^2\theta\ \sin(2\theta) \quad (3)$$

$$I^{\perp}(A_{1g}) \propto 1/4[|a|^2 + |b|^2 - 2\ \mathrm{Re}|a\cdot b^*|]\ \sin^2(2\theta) \quad (4)$$

$$I^{\perp}(E_g) \propto 1/4|c|^2\sin^2(2\theta) + |d|^2\cos^2(2\theta) + 1/2\ \mathrm{Re}(c\cdot d^*)\ \sin(4\theta) \quad (5)$$

The angular-dependent Raman intensities of different vibrating modes of the β-As monolayer for four laser lines 532, 633, 785, and 830 nm are shown in Figure 2 (parallel polarization configuration) and Figure 3 (perpendicular polarization configuration). The order of magnitude of

DOI: 10.1021/acsomega.9b00712
ACS Omega 2019, 4, 10171−10175

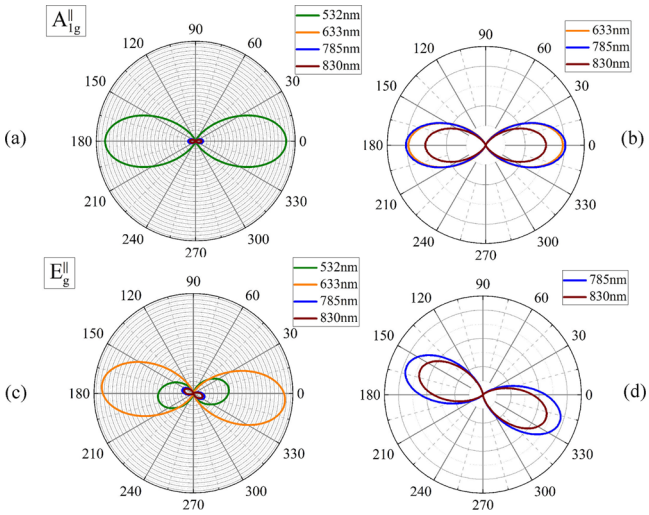

Figure 2. Polar plots of the angular-dependent Raman intensities, $|\vec{e}_s \cdot \vec{R} \cdot \vec{e}_i|^2$, of A_{1g} mode (a) and E_g mode (c) of the β-As monolayer for four laser lines 532 nm (green), 633 nm (orange), 785 nm (red), and 830 nm (wine). The plots corresponding to the latter three and two laser lines are enlarged in (b) for the A_{1g} mode and (d) for the E_g mode, respectively. The polarization direction of the scattered light is parallel to the polarization direction of the incident light. The incident and scattered light are in x-direction.

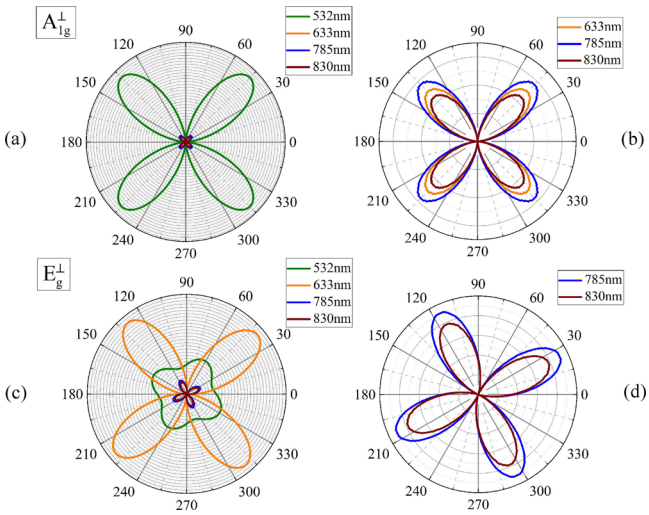

Figure 3. Polar plots of the angular-dependent Raman intensities, $|\vec{e}_s \cdot \vec{R} \cdot \vec{e}_i|^2$, of the A_{1g} mode (a) and E_g mode (c) of the β-As monolayer for 532 nm (green), 633 nm (orange), 785 nm (red), and 830 nm (wine). The plots corresponding to the latter three and two laser lines are enlarged in (b) for the A_{1g} mode and (d) for E_g mode, respectively. The polarization direction of the scattered light is perpendicular to the polarization direction of the incident light. The incident and scattered light are in x-direction.

Raman intensities is different because the Raman intensity is proportional to ω_s^4 (eq 11 in the Methods section). Therefore, we plot $|\vec{e}_s \cdot \vec{R} \cdot \vec{e}_i|^2$ for clarity. Raman intensities of the A_{1g} and E_g modes in parallel polarization configurations have two maxima for all of the laser lines (Figure 2). The first term is dominant in eq 2 because $|a| \gg |b|$. Therefore, the maxima locate at θ = 0° and 180° for the A_{1g} mode; the minima intensities are zero at θ = 90° and 270° for the A_{1g} mode. The first term and the third term in eq 3 are dominant because $|c| \approx 2|d|$. Therefore, the common factor $\cos^2\theta$ of these two terms leads to the similarity of the polar plots of the E_g mode and that of the A_{1g} mode. The remaining factors in eq 3 rotate the polar plots of the E_g mode with respect to that of the A_{1g} mode.

We did not find a configuration that has four maxima as blue phosphorene had in the parallel polarization configuration.[24]

In the perpendicular polarization configuration, both the A_{1g} and E_g modes have four maxima for all of the laser lines. The common factor $\sin^2(2\theta)$ in eq 4 determines that the four maxima of all of the laser lines locate at $\theta = 45° + n\,90°$ for the A_{1g} mode; the minima intensities are zero at $\theta = n\,90°$ for the A_{1g} mode, where n is an integer. This is not relevant to the relative value of a and b. The summary of the first two terms in eq 5 is approximately a constant $|d|^2$ because $|c| \approx 2|d|$ for laser lines 830, 785, and 532 nm. Therefore, the location of maxima and minima of polar plots of the E_g mode is determined by the third term. The minima (maxima) locate near $67.5° + n\,90°$ ($22.5° + n\,90°$) because the difference of argument of c and d is less than $\pi/2$ for laser lines 830 and 785 nm. The minima (maxima) locate near $22.5° + n\,90°$ ($67.5° + n\,90°$) because the difference of argument of c and d is larger than $\pi/2$ for the laser line 532 nm. The difference of argument of c and d is close to $\pi/2$ for the laser line 532 nm. Therefore, the third term in eq 5 is small; thus, the minimal amplitude of the polar plots of the E_g mode is close to the maximal amplitude, which is distinctly different from other polar plots. For the laser line 633 nm, the first term in eq 5 is dominant because $|c| \gg |d|$. Therefore, the minima (maxima) locate near $n\,90°$ ($45° + n\,90°$).

When the incident light is perpendicular to the plane of β-As, the polarization direction can be written as $e_i = (\cos\theta, \sin\theta, 0)$. Then, the polarization direction of the parallel and perpendicular polarized scattered light is $e_s^{\parallel} = (\cos\theta, \sin\theta, 0)$ and $e_S^{\perp} = (-\sin\theta, \cos\theta, 0)$, respectively. The Raman intensities of the parallel and perpendicular polarized scattered light are

$$I^{\parallel}(A_{1g}) \propto |a|^2 \tag{6}$$

$$I^{\parallel}(E_g) \propto |c|^2 \tag{7}$$

$$I^{\perp}(A_{1g}) = 0 \tag{8}$$

$$I^{\perp}(E_g) \propto |c|^2 \tag{9}$$

As one can see in the equations, only two elements of the Raman tensor (a and c) play the role in the Raman intensity, whereas the Raman intensity depends on all elements of the Raman tensor when the incident light is parallel with the plane. In addition, the Raman intensity of the A_{1g} mode for parallel polarized scattered light depends only on a; it is zero for perpendicular polarized scattered light. The Raman intensity of E_g mode depends only on c. None of the Raman intensities depend on the polarization angle θ.

The phonon frequencies are 7.05 and 9.14 THz for the in-plane (E_g) and out-of-plane (A_{1g}) vibration modes at Γ point, respectively. Therefore, there are two peaks (235 and 305 cm^{-1}) in the nonresonant Raman spectra (Figure 4). As listed in Table 1, it is similar to germanene,[30] blue phosphorene,[24] and β-Sb monolayer.[25] The Raman intensity corresponding to the E_g mode is stronger than that corresponding to the A_{1g} mode for the β-As monolayer except for laser line 633 nm. The Raman intensity for different laser lines follows hierarchy $I_{532} > I_{633} > I_{785} > I_{830}$ except I_{633} of the E_g mode.

DOI: 10.1021/acsomega.9b00712
ACS Omega 2019, 4, 10171−10175

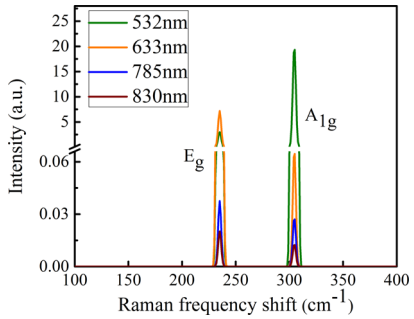

Figure 4. Nonresonant Raman spectra of the β-As monolayer for four laser lines: 532 nm (green), 633 nm (orange), 785 nm (red), and 830 nm (wine). There are two peaks at 305 cm^{-1} (A_{1g} mode) and 235 cm^{-1} (E_g mode).

We also calculate the absorbance of the β-As monolayer (Figure 5). The absorbance is isotropic for lights with polarization direction in the $x-y$ plane. The absorbance increases with the photon energy for the four laser lines we concerned.

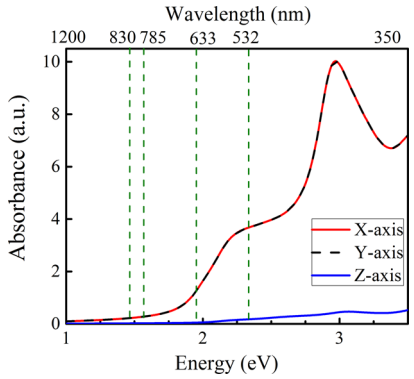

Figure 5. Absorbance spectra of the β-As monolayer for incident light with polarization direction in x (red), y (black dash), and z (blue) directions. The four vertical green dashed lines indicate the photon energy of four laser lines 830 nm (1.49 eV), 785 nm (1.57 eV), 633 nm (1.96 eV), and 532 nm (2.33 eV).

CONCLUSIONS

In summary, we systematically investigated vibrational properties and Raman spectra of the buckled gray arsenic (β-As monolayer) for four commonly used laser lines 532, 633, 785, and 830 nm. There are not any imaginary vibrating modes, which mean the β-As monolayer has the dynamic stability. All of the optical modes are Raman active. The calculated Raman spectra show that there are two peaks at 235 and 305 cm^{-1} where the former one corresponds to degenerate in-plane vibration modes E_g and the latter corresponds to the out-of-plane vibration mode A_{1g}. We calculated polarization angle-dependent Raman intensities when the wave vector of incident light is parallel and perpendicular to the plane of the β-As monolayer. There are two (four) minima and two (four) maxima when the polarization direction of scattered light is parallel (perpendicular) to that of incident light and the wave vector of the incident light is parallel to the β-As monolayer. The Raman intensities of neither parallel polarization configuration nor perpendicular polarization configuration depend on the polarization direction when the wave vector of incident light is perpendicular to the β-As monolayer. The shapes of the polar plots are resulted from the argument difference between Raman tensor elements (c and d) and relative amplitudes of Raman tensor elements ($|a| \gg |b|$ and $|c| \approx 2|d|$). The Raman intensities decrease with increasing wavelength of incident laser line except that of the E_g mode for laser line 633 nm.

METHODS

Geometry optimization and dielectric tensor calculation are done with Vienna Ab initio Simulation Package.[31] Phonon frequency and phonon modes are obtained with Phonopy code.[32] The exchange−correlation potential is treated at the level of the generalized gradient approximation using Perdew−Burke−Ernzerhof.[33] For constructing basis set, the projected augmented wave method[34,35] is employed. Energy cutoff for all calculations is 500 eV. The Brillouin zone of the unit cell structure is sampled with a 15 × 15 × 1 and 40 × 40 × 1 k-point grid for geometry optimization and static calculation, respectively. Vacuum slabs of 1.5 nm thick are inserted between neighboring 2D atom sheets. The convergence tolerance for the total energy and force calculations set to 10^{-7}eV and 0.01 eV/Å, respectively.

The Raman tensor is obtained with a finite displacement method[36−38]

$$R_{\alpha\beta}(j) = V\sum_{\mu=1}^{N}\sum_{l=1}^{3}\frac{\partial\chi_{\alpha\beta}}{\partial r_l(\mu)}\frac{e_l^j(\mu)}{\sqrt{M_\mu}} \quad (10)$$

where V is the volume of unit cell, M_μ is the atomic mass of atom μ, and $\delta\chi_{\alpha\beta}/\delta r_l(\mu)$ is the first derivative of the electric polarizability tensor with respect to the atomic displacement. It equals with the derivative of dielectric tensor $\varepsilon_{\alpha\beta}$ divided by 4π because $\chi_{\alpha\beta}(\omega) = (\varepsilon_{\alpha\beta}(\omega) - \delta_{\alpha\beta})/4\pi$. ω is the frequency of laser electric field. $e_l^j(\mu)$ is the eigen vector of the j-th phonon mode at Γ point. The dielectric tensor of the structure with finite displacement can be obtained with DFT.

Then, the Raman intensity can be obtained[36−38]

$$I \propto \omega_s^4|\vec{e}_s\cdot\vec{R}\cdot\vec{e}_i|^2 \quad (11)$$

where ω_s is the frequency of scattered light, $\vec{e}_i$ and $\vec{e}_s$ are electric polarization vectors of incident and scattered light, respectively.

AUTHOR INFORMATION

Corresponding Authors

*E-mail: stslzb@mail.sysu.edu.cn (Z.L.).
*E-mail: wangwl2@mail.sysu.edu.cn (W.W.).

ORCID

Somayeh Saboori: 0000-0002-9130-1217
Weiliang Wang: 0000-0002-8330-9913
Juncong She: 0000-0002-5483-3636

Notes

The authors declare no competing financial interest.

ACKNOWLEDGMENTS

This work was supported by the National R&D Key Plan Project of China (2016YFA0202000), National Natural Science Foundation of China (grant no. 11604391 and 61874144), the Guangzhou Science Technology and Innovation Commission (grant no. 201607020012), Special Program for Applied Research on Super Computation of the NSFC-Guangdong Joint Fund (the second phase), and the high-

DOI: 10.1021/acsomega.9b00712
ACS Omega 2019, 4, 10171−10175

performance grid computing platform of Sun Yat-sen University.

REFERENCES

(1) Hong, T.; Chamlagain, B.; Lin, W.; Chuang, H.-J.; Pan, M.; Zhou, Z.; Xu, Y.-Q. Polarized photocurrent response in black phosphorus field-effect transistors. *Nanoscale* **2014**, *6*, 8978−8983.
(2) Chen, M.; Yu, Z.; Wang, Y.; Xie, Y.; Wang, J.; Guo, H. Nonequilibrium spin injection in monolayer black phosphorus. *Phys. Chem. Chem. Phys.* **2016**, *18*, 1601−1606.
(3) Liu, J.; Choi, G.-M.; Cahill, D. G. Measurement of the anisotropic thermal conductivity of molybdenum disulfide by the time-resolved magneto-optic Kerr effect. *J. Appl. Phys.* **2014**, *116*, 233107.
(4) Zhang, J. L.; Zhao, S.; Han, C.; Wang, Z.; Zhong, S.; Sun, S.; Guo, R.; Zhou, X.; Gu, C. D.; Yuan, K. D.; Li, Z.; Chen, W. Epitaxial Growth of Single Layer Blue Phosphorus: A New Phase of Two-Dimensional Phosphorus. *Nano Lett.* **2016**, *16*, 4903−4908.
(5) Zhang, J.; Liu, H. J.; Cheng, L.; Wei, J.; Liang, J. H.; Fan, D. D.; Jiang, P. H.; Shi, J. Thermal conductivities of phosphorene allotropes from first-principles calculations: a comparative study. *Sci. Rep.* **2017**, *7*, 4623.
(6) Zhu, Z.; Tomanek, D. Semiconducting Layered Blue Phosphorus: A Computational Study. *Phys. Rev. Lett.* **2014**, *112*, 6802.
(7) Sun, M.; Wang, S.; Yu, J.; Tang, W. Hydrogenated and halogenated blue phosphorene as Dirac materials: A first principles study. *Appl. Surf. Sci.* **2017**, *392*, 46−50.
(8) Zheng, H.; Yang, H.; Wang, H.; Du, X.; Yan, Y. Electronic and magnetic properties of nonmetal atoms doped blue phosphorene: First-principles study. *J. Magn. Magn. Mater.* **2016**, *408*, 121−126.
(9) Lei, T.; Liu, C.; Zhao, J.-L.; Li, J.-M.; Li, Y.-P.; Wang, J.-O.; Wu, R.; Qian, H.-J.; Wang, H.-Q.; Ibrahim, K. Electronic structure of antimonene grown on Sb2Te3 (111) and Bi2Te3 substrates. *J. Appl. Phys.* **2016**, *119*, 015302.
(10) Shekar, S. C.; Swathi, R. S. Stability of Nucleobases and Base Pairs Adsorbed on Graphyne and Graphdiyne. *J. Phys. Chem. C* **2014**, *118*, 4516−4528.
(11) Vogt, P.; De Padova, P.; Quaresima, C.; Avila, J.; Frantzeskakis, E.; Asensio, M. C.; Resta, A.; Ealet, B.; Le Lay, G. Silicene: Compelling Experimental Evidence for Graphenelike Two-Dimensional Silicon. *Phys. Rev. Lett.* **2012**, *108*, 5501.
(12) Norman, N. C. *Chemistry of Arsenic, Antimony and Bismuth*; Springer, 1998; ISBN. 978-0-7514-0389-3, p 50.
(13) Kamal, C.; Ezawa, M. Arsenene: Two-dimensional buckled and puckered honeycomb arsenic systems. *Phys. Rev. B: Condens. Matter Mater. Phys.* **2015**, *91*, 5423.
(14) Kecik, D.; Durgun, E.; Ciraci, S. Optical properties of single-layer and bilayer arsenene phases. *Phys. Rev. B* **2016**, *94*, 5410.
(15) Zhu, Z.; Guan, J.; Tomanek, D. Strain-induced metal-semiconductor transition in monolayers and bilayers of gray arsenic: A computational study. *Phys. Rev. B* **2015**, *91*, 1404.
(16) Madelung, O. *Semiconductors: Data Handbook*, 3rd; Springer-Verlag: New York, 2004; p 405.
(17) Tsai, H.-S.; Wang, S.-W.; Hsiao, C.-H.; Chen, C.-W.; Ouyang, H.; Chueh, Y.-L.; Kuo, H.-C.; Liang, J.-H. Direct Synthesis and Practical Bandgap Estimation of Multilayer Arsenene Nanoribbons. *Chem. Mater.* **2016**, *28*, 425−429.
(18) Zhang, S.; Yan, Z.; Li, Y.; Chen, Z.; Zeng, H. Atomically Thin Arsenene and Antimonene: Semimetal-Semiconductor and Indirect-Direct Band-Gap Transitions. *Angew. Chem. Int. Ed.* **2015**, *54*, 3112−3115.
(19) Yuanfeng, X.; Bo, P.; Hao, Z.; Hezhu, S.; Rongjun, Z.; Hongliang, L.; Zhang, D. W.; Heyuan, Z., First-principle calculations of phononic, electronic and optical properties of monolayer arsenene and antimonene allotropes. arXiv, **2017**; Vol *17*, p 17.
(20) Zhang, Z.; Xie, J.; Yang, D.; Wang, Y.; Si, M.; Xue, D. Manifestation of unexpected semiconducting properties in few-layer orthorhombic arsenene. *Appl. Phys. Express* **2015**, *8*, 055201.
(21) Ambrosi, A.; Sofer, Z.; Pumera, M. Electrochemical Exfoliation of Layered Black Phosphorus into Phosphorene. *Angew. Chem. Int. Ed.* **2017**, *56*, 10443−10445.
(22) Yuan, J.; Zhao, M.; Yu, W.; Lu, Y.; Chen, C.; Xu, M.; Li, S.; Loh, K.; Qiaoliang, B. Raman Spectroscopy of Two-Dimensional Bi2TexSe3-x Platelets Produced by Solvothermal Method. *Materials* **2015**, *8*, 5007−5017.
(23) Ouyang, G.; Sun, C. Q.; Zhu, W.-G. Pressure-stiffened Raman phonons in group III nitrides: A local bond average approach. *J. Phys. Chem. B* **2008**, *112*, 5027−5031.
(24) Deng, Z.; Li, Z.; Wang, W.; She, J. Vibrational properties and Raman spectra of pristine and fluorinated blue phosphorene. *Phys. Chem. Chem. Phys.* **2019**, *21*, 1059−1066.
(25) Wang, G.; Pandey, R.; Karna, S. P. Atomically Thin Group V Elemental Films: Theoretical Investigations of Antimonene Allotropes. *ACS Appl. Mater. Interfaces* **2015**, *7*, 11490−11496.
(26) Kou, L.; Ma, Y.; Tan, X.; Frauenheim, T.; Du, A.; Smith, S. Structural and Electronic Properties of Layered Arsenic and Antimony Arsenide. *J. Phys. Chem. C* **2015**, *119*, 6918−6922.
(27) Yang, W.; Cohen, A. J.; Mori-Sanchez, P. Derivative discontinuity, bandgap and lowest unoccupied molecular orbital in density functional theory. *J. Chem. Phys.* **2012**, *136*, 204111.
(28) Zheng, X.; Cohen, A. J.; Mori-Sanchez, P.; Hu, X.; Yang, W. Improving Band Gap Prediction in Density Functional Theory from Molecules to Solids. *Phys. Rev. Lett.* **2011**, *107*, 6403.
(29) Martin, R.; Falicov, L. *Light scattering in solids*; Topics in Applied Physics; Springer-Verlag Berlin Heidelberg, 1975; Vol *8*, p XIII, 342, xiii+79 pp-xiii+149.
(30) Lazzeri, M.; Mauri, F. First-principles calculation of vibrational Raman spectra in large systems: Signature of small rings in crystalline SiO2. *Phys. Rev. Lett.* **2003**, *90*, 6401.
(31) Kresse, G.; Furthmüller, J. Efficient iterative schemes for ab initio total-energy calculations using a plane-wave basis set. *Phys. Rev. B: Condens. Matter Mater. Phys.* **1996**, *54*, 11169−11186.
(32) Togo, A.; Chaput, L.; Tanaka, I.; Hug, G. First-principles phonon calculations of thermal expansion in Ti3SiC2, Ti3AlC2, and Ti3GeC2. *Phys. Rev. B: Condens. Matter Mater. Phys.* **2010**, *81*, 4301.
(33) Perdew, J. P.; Chevary, J. A.; Vosko, S. H.; Jackson, K. A.; Pederson, M. R.; Singh, D. J.; Fiolhais, C. Atoms, molecules, solids, and surfaces: Applications of the generalized gradient approximation for exchange and correlation. *Phys. Rev. B: Condens. Matter Mater. Phys.* **1992**, *46*, 6671−6687.
(34) Blöchl, P. E. Projector augmented-wave method. *Phys. Rev. B: Condens. Matter Mater. Phys.* **1994**, *50*, 17953−17979.
(35) Kresse, G.; Joubert, D. From ultrasoft pseudopotentials to the projector augmented-wave method. *Phys. Rev. B* **1999**, *59*, 1758−1775.
(36) Ceriotti, M.; Pietrucci, F.; Bernasconi, M. Ab initio study of the vibrational properties of crystalline TeO2: The alpha, beta, and gamma phases. *Phys. Rev. B* **2006**, *73*, 4304.
(37) Liang, L.; Meunier, V. First-principles Raman spectra of MoS2, WS2 and their heterostructures. *Nanoscale* **2014**, *6*, 5394−5401.
(38) Umari, P.; Pasquarello, A.; Dal Corso, A. Raman scattering intensities in alpha-quartz: A first-principles investigation. *Phys. Rev. B: Condens. Matter Mater. Phys.* **2001**, *63*, 4305.

DOI: 10.1021/acsomega.9b00712
ACS Omega 2019, 4, 10171−10175